

FAST-Splat: Fast, Ambiguity-Free Semantics Transfer in Gaussian Splatting

Ola Shorinwa Jiankai Sun Mac Schwager
Stanford University

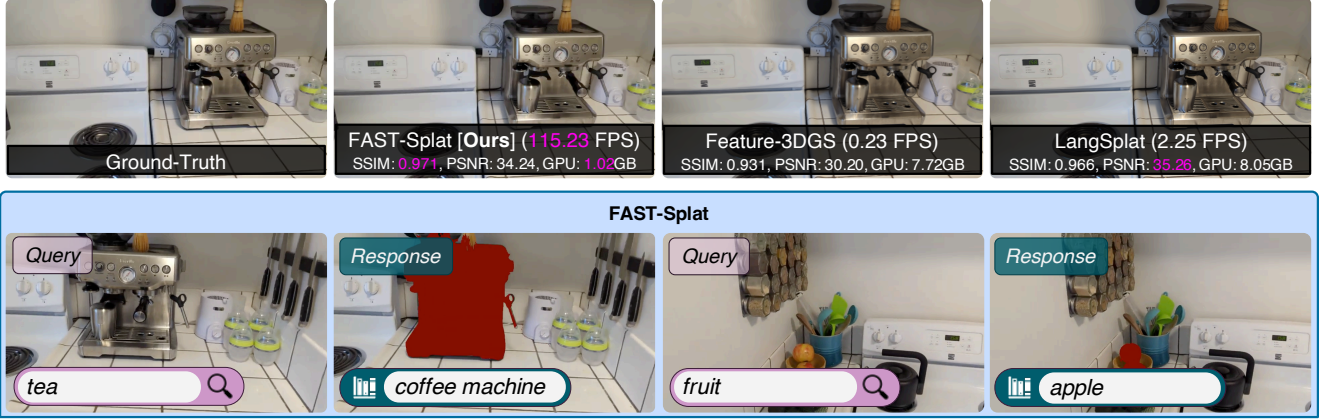


Figure 1. FAST-Splat enables fast, ambiguity-free semantic Gaussian Splatting, achieving 6x to 8x faster training times, 18x to 51x faster rendering speeds, and 6x lower GPU memory usage compared to prior work. FAST-Splat resolves language/scene-attributed ambiguity in object localization, providing the precise semantic label of objects when given a user query, e.g., in the illustrated cases with a related but different object, FAST-Splat informs a user that it found a *coffee machine* given the query: “tea,” and an *apple* given the query: “fruit.”

Abstract

We present FAST-Splat for fast, ambiguity-free semantic Gaussian Splatting, which seeks to address the main limitations of existing semantic Gaussian Splatting methods, namely: slow training and rendering speeds; high memory usage; and ambiguous semantic object localization. We take a bottom-up approach in deriving FAST-Splat, dismantling the limitations of closed-set semantic distillation to enable open-set (open-vocabulary) semantic distillation. Ultimately, this key approach enables FAST-Splat to provide precise semantic object localization results, even when prompted with ambiguous user-provided natural-language queries. Further, by exploiting the explicit form of the Gaussian Splatting scene representation to the fullest extent, FAST-Splat retains the remarkable training and rendering speeds of Gaussian Splatting. Precisely, while existing semantic Gaussian Splatting methods distill semantics into a separate neural field or utilize neural models for dimensionality reduction, FAST-Splat directly augments each Gaussian with specific semantic codes, preserving the training, rendering, and memory-usage advantages of Gaussian Splatting over neural field methods. These Gaussian-specific semantic codes, together with a hash-table, enable semantic similarity to

be measured with open-vocabulary user prompts and further enable FAST-Splat to respond with unambiguous semantic object labels and 3D masks, unlike prior methods. In experiments, we demonstrate that FAST-Splat is 6x to 8x faster to train, achieves between 18x to 51x faster rendering speeds, and requires about 6x smaller GPU memory, compared to the best-competing semantic Gaussian Splatting methods. Further, FAST-Splat achieves relatively similar or better semantic segmentation performance compared to existing methods. After the review period, we will provide links to the project website and the codebase.

1. Introduction

Research breakthroughs in vision-language foundation models have underpinned the remarkable performance of state-of-the-art object detection and classification [24, 51], segmentation [16, 29], and image captioning [27, 44]. In general, these models learn useful multi-modal image-language representations, entirely supervised with 2D image-text pairs, all within a shared representation space. Recent work has shown that grounding the semantic knowledge encoded by vision-language foundation models in 3D can be useful in improving semantic segmentation and localization [13, 35]

(especially in models that take in low-resolution images as input), enabling applications such as 3D scene-editing [15, 40] and robotic manipulation [28, 36]. Although these methods demonstrate compelling object segmentation performance from open-vocabulary queries, these methods fail to disambiguate between the semantic classes of unique objects that are semantically-similar to the natural language query [13]. For example, when a user queries specifically for “tea,” existing semantic Gaussian Splatting (GSplat) methods localize the coffee machine without providing any clarifying information on the identity of the localized object, suggesting that “tea” exists in the scene, when the contrary is true. This ambiguity generally arises from the fact that many vision-language foundation methods, e.g., CLIP, utilize a bag-of-words approach in measuring the semantic similarity between image-language queries. Moreover, many semantic methods for Gaussian Splatting are notably slow, requiring a significant amount of memory and computation time for training and inference. We seek to derive a semantic GSplat method that addresses these limitations.

In this work, we propose FAST-Splat, a *Fast, Ambiguity-free Semantics Transfer* method for Gaussian Splatting. FAST-Splat generates fine-grained semantic localization, with highly specific semantic classes even in the presence of ambiguous natural-language prompts, and as its name implies, runs much faster than existing semantic GSplat methods. FAST-Splat utilizes the vision-language foundation model CLIP [27] to embed open-set semantics into GSplat models, enabling optional initialization of relevant objects from closed-set object detectors. However, noting the limited coverage of closed-set object detectors, FAST-Splat leverages open-set object detectors and segmentation models to enable queryable semantics from free-form natural language, illustrated in Figure 2. By constructing a hash-table of identified objects, FAST-Splat enables effective semantic disambiguation, while addressing the weaknesses of closed-set methods. To enable significantly faster training and rendering speeds compared to prior work, FAST-Splat implements two key innovations: (i) single-phase semantic distillation and (ii) neural-free semantic radiance fields. FAST-Splat distills semantics into the underlying GSplat model for scene reconstruction using a single-phase training procedure, simultaneously training the geometric, visual, and semantic components of the GSplat model. In contrast, prior work, e.g., [26], utilizes a two-phase training procedure, training the geometric and visual components of the scene before introducing and optimizing the semantic parameters, negatively impacting computational performance. Moreover, unlike existing semantic GSplat methods which rely on neural-field models for semantic distillation, FAST-Splat directly augments each Gaussian with specific semantic codes, without any neural model. These key insights not only enable FAST-Splat to exploit the explicit

scene-representation of Gaussian Splatting for faster training and rendering speeds, but also enable FAST-Splat to provide unambiguous semantic object labels in response to open-vocabulary user queries, e.g., in semantic object localization, upon identifying semantically-similar objects using the semantic codes associated with each Gaussian, along with the semantic hash-table.

We compare FAST-Splat to existing semantic GSplat methods [26, 50] on standard benchmark datasets. FAST-Splat achieves 6x to 8x faster training times and 18x to 51x faster rendering speeds, while requiring 6x smaller GPU memory. Meanwhile, FAST-Splat achieves competitive or better semantic object localization performance. Notably, FAST-Splat enables semantic disambiguation in object localization, even with ambiguous user-provided natural-language queries, which we illustrate in Figure 1. In contrast to prior work, FAST-Splat provides a clarifying semantic label to each localized object, disambiguating the semantic identity of the localized object. For example, in Figure 1, when prompted with the query “tea,” FAST-Splat notifies a user that it localized a *coffee machine*, and an *apple* when given the query: “fruit.” Such disambiguation can be critical to enabling interesting downstream applications, e.g., in robotics.

To summarize our contributions:

- We introduce FAST-Splat, a Fast, Ambiguity-Free Semantic GSplat method that enables notably faster (6x to 8x faster) language-semantics grounding in 3D scenes, distilled from 2D vision models.
- FAST-Splat resolves semantic ambiguity in semantic object localization, arising from ambiguous user-provided natural-language queries or inherent scene ambiguity, enabling the identification of the precise semantic label of relevant objects.
- FAST-Splat achieves superior rendering speeds for semantic Gaussian Splatting, about 18x to 51x faster rendering speeds compared to prior work.

2. Related Work

We provide a detailed review of existing work on open-vocabulary object detection and segmentation, along with follow-on work on grounding 2D object detection and segmentation in 3D by leveraging high-fidelity 3D scene representations.

Open-Vocabulary Object Detection and Segmentation.

The introduction of the vision transformer (ViT) architecture [7] has spurred rapid research advances in many classical computer vision tasks, such as object detection and segmentation. However, like their convolutional neural network (CNN) counterparts [9, 31], early ViT models [3, 46] were primarily trained to detect objects within a fixed number of classes, defined as closed-set object detection. Vision-image foundation models, e.g., CLIP [27] and transformer-based

language encoders, such as BERT [6], have enabled the detection of objects through open-vocabulary natural-language prompts, without relying on a fixed number of object classes, referred to as open-set object detection. Open-vocabulary object detection methods [8, 18, 22, 24, 45] fuse the image and language embeddings from vision or language foundation models using a decoder transformer architecture with self-attention to detect objects in a query image. GLIP [18] and OWL-ViT [24] train an image and text encoder jointly to learn useful representations, which are fed to a decoder for 2D grounding. While GLIP and OWL-ViT require a pretraining phase on large-scale internet image-text pairs, GroundingDINO [22] leverages pre-trained text encoder BERT [6], but otherwise utilizes a similar model architecture.

Zero-shot object segmentation methods [17, 21, 29, 42] leverage an encoder-decoder model architecture to generate a semantic mask of all instances of objects in an image. Mask DINO [17] introduces a mask prediction branch to DINO [46], extending it to object segmentation. Like GLIP, ViL-Seg [21] trains an image and text encoder together with a clustering head on image-caption pairs gathered on the internet to segment objects, enabling segmentation from natural-language prompts. SAM-2 [29] utilizes an image encoder with memory attention and a memory bank to enable video segmentation (in addition to image segmentation). However, SAM requires a mask, bounding box, or pixel-coordinate prompt for segmentation. GroundedSAM [32] extends SAM-2 to open-vocabulary queries by computing the bounding box associated with a given natural-language query, which is passed as an input prompt to SAM-2. Other methods [16, 19, 47] leverage pre-trained image and text encoders, which are fine-tuned in some cases, to enable open-vocabulary object segmentation.

Radiance Fields. Neural Radiance Fields (NeRFs) [1, 23, 25] represent a scene as a color and density field, parameterized by multi-layer perceptrons. NeRFs generate a photorealistic reconstruction of a scene, capturing high-fidelity visual details. However, high-quality NeRFs typically require long training times and achieve slow rendering rates. Gaussian Splatting [12] addresses these limitations by representing a scene using ellipsoidal primitives with visual attributes, such as opacity and color using spherical harmonics, in addition to the spatial and geometric attributes, such as the ellipsoid’s mean and covariance. Radiance fields can be trained entirely from RGB images, making them suitable for many vision tasks.

Grounding Language in 3D. To bridge the gap between 2D object detection and 3D object localization, prior work has examined grounding semantic embeddings from pre-trained image and text encoders in the 3D world. CLIP-Fields [35] learns an implicit spatial mapping from 3D points to CLIP image embeddings and Sentence-Bert [30] text embeddings using back-projected RGB-D points. VLMaps [11] and

NLMap [4] distill vision-language features into grid-based maps. The sparsity of these maps limits the resolution of the open-vocabulary segmentation results achievable by these methods. For high-resolution object segmentation, Distilled Features Fields (DFF) [15], CLIP-NeRF [40], and LERF [13] ground CLIP [27], LSeg [16], and DINO [46] features in a NeRF representation of the scene. Moreover, similar techniques have been employed in [10, 26, 50, 52] to distill semantic features into GSplat representations. The resulting distilled radiance fields (DRFs) enable dense open-vocabulary object segmentation in 3D and have been applied to scene-editing [15, 40] and robotic mapping and manipulation [28, 36–38, 49]. Despite their success in object segmentation, existing DRFs fail to precisely identify the semantic class of the segmented object, e.g., for a given query, these methods localize all objects related to the query without resolving the unique semantic identity of each object. This ambiguity creates a gap in scene understanding, which is often required in many downstream tasks, e.g., in robotic exploration or manipulation. In this work, we introduce a DRF with fine-grained semantics, enabling precise semantic identification of objects in a scene, disambiguating language-guided semantic object localization, and addressing existing challenges.

3. Preliminaries

Here, we provide some background information on Gaussian Splatting. Gaussian Splatting [12] represents a scene using ellipsoidal primitives, with ellipsoid i parameterized by its mean $\mu_i \in \mathbb{R}^3$; covariance $\Sigma = RSS^T R^T \in \mathbb{R}^{3 \times 3}$, where R denotes a rotation matrix, and S denotes a diagonal scaling matrix; opacity α ; and spherical harmonics (SH). Gaussian Splatting utilizes a tile-based rasterization procedure for efficient real-time rendering rates, outperforming NeRF-based representations, with the color C of each pixel given by the α -based blending procedure:

$$C = \sum_{i \in \mathcal{N}} c_i \alpha_i \prod_{j=1}^i (1 - \alpha_j), \quad (1)$$

where c_i denotes the color of each ellipsoid and α_i denotes the per-ellipsoid opacity multiplied by the probability density of the 2D Gaussian associated with the ellipsoid. Upon initialization from a sparse point cloud, which can be obtained from structure-from-motion, the attributes of each ellipsoid are optimized through gradient descent on a dataset of RGB images. Distilled feature fields build upon NeRFs and Gaussian Splatting, leveraging the same volumetric rendering and tile-based rasterization for NeRFs and Gaussian Splatting, respectively, to generate 2D feature maps from the 3D feature fields.

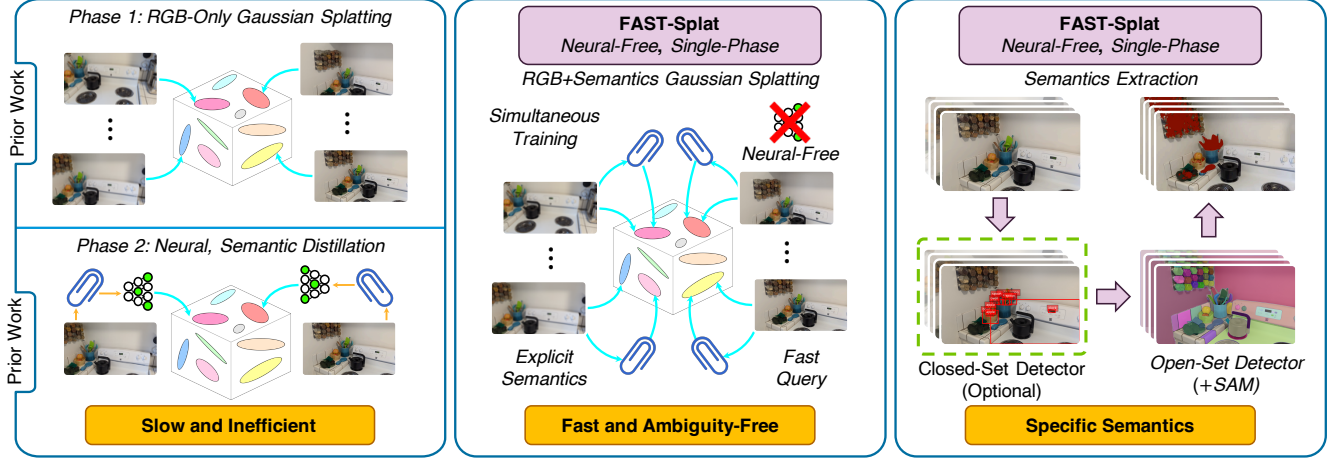


Figure 2. Unlike prior semantic Gaussian Splatting methods, FAST-Splat jointly optimizes the geometric, visual, and semantic attributes of Gaussian Splatting models, achieving faster training and rendering times with effective semantics disambiguation using an efficient semantics extraction procedure.

4. Fast, Ambiguity-Free Semantic Transfer

Now, we discuss FAST-Splat, a fast, fine-grained semantic distillation method for grounding 2D language semantics in 3D, enabling precise identification of the semantic label of objects in the 3D scenes. We build off 3D Gaussian Splatting to obtain a high-fidelity, photorealistic scene reconstruction entirely from RGB images. Given a dataset of images \mathcal{D} , Gaussian Splatting optimizes the mean, covariance, opacity, and SH parameters of each ellipsoid comprising the representation via the loss function:

$$\mathcal{L}_{\text{gs}} = (1 - \lambda) \sum_{\mathcal{I} \in \mathcal{D}} \|\mathcal{I} - \hat{\mathcal{I}}\|_1 + \lambda \mathcal{L}_{\text{D-SSIM}}, \quad (2)$$

where $\lambda \in [0, 1]$ denotes a weighting parameter between the ℓ_1 -loss term and the differentiable structural similarity index measure (D-SSIM) loss term, and \mathcal{I} and $\hat{\mathcal{I}}$ denote the ground-truth and predicted RGB image, respectively. The GSplat model is trained using the Adam optimizer [14], a gradient-based optimization method.

Almost all existing semantic distillation methods rely on neural architectures for grounding language in 3D in NeRFs [13, 15, 40] and GSplat scenes [10, 26, 50, 52]. Although effective in enabling open-set semantic object localization, neural-based approaches introduce significant computational bottlenecks into the training pipeline of NeRF and GSplat scenes. In particular, when utilized in Gaussian Splatting, neural-based semantic distillation essentially erases the computational gains, e.g., faster training times and rendering rates, afforded by Gaussian Splatting when compared to NeRFs. Moreover, prior semantic GSplat methods, e.g., [26], train the semantic attributes of a scene independently from its geometric and visual attributes, utilizing a two-phase training procedure, where the geometric and visual attributes

are first optimized before the semantic attributes. This training framework significantly increases the time required for training GSplat models. We contrast this training framework with the training framework utilized by FAST-Splat, which implements a single-phase training procedure, jointly optimizing all attributes of the scene, in Figure 2.

Via FAST-Splat, we seek to derive a method for open-set semantic distillation, while preserving the faster training times and rendering rates achieved by the underlying GSplat method. To achieve this goal, we revisit the fundamental insight exploited by the authors of the original GSplat work [12], namely: that only representing occupied space explicitly can lead to significant speedup in training and rendering times without any notable degradation in the visual fidelity of the representation. Specifically, Gaussian Splatting harnesses the explicit form and sparsity of an ellipsoidal-primitive-based scene representation to achieve faster training times and rendering times compared to NeRFs, the state-of-the-art at the time, which relied on implicit fields for the color and density of the scene. By learning neural encoders for dimensionality reduction or neural fields for language semantics, existing semantic distillation methods for Gaussian Splatting fail to take advantage of this insight. In contrast, in FAST-Splat, we leverage this insight to speed up training and rendering times, by eschewing neural models. In particular, we augment the attributes of each ellipsoid with a semantic parameter, associated with its semantic identity $\beta \in \mathbb{R}^3$, which is trained simultaneously with the ellipsoid’s other attributes. Note that the dimension of β does not pose a limitation unique to this work. In fact, existing semantic GSplat methods, e.g., [26], generally use three-dimensional semantic codes to enable the utilization of the rasterization procedure employed in Gaussian Splatting.

Closed-Set Semantic Gaussian Splatting. FAST-Splat supports initialization of the semantics extraction procedure using closed-set object detectors. To obtain the closed-set semantic categories, we feed each image $I \in \mathcal{D}$ into an object detector, e.g., YOLO [41], DETR [3], and Efficient DETR [43], to generate a list of objects present in the image. Although closed-set object detectors generally exhibit remarkable performance, these detectors occasionally fail to identify all instances of an object in an image, given that the size of their dictionary of detectable objects is often limited. To overcome this challenge, FAST-Splat utilizes an open-set detector, e.g., GroundingDINO [22], with input prompts from, e.g., image-tagging models [48] or closed-set object detectors. We examine the importance of the open-set object detector in ablations in the experiments in Section 5.

At this stage, each image has a list of constituent objects and bounding boxes specifying the location of these objects in the image. However, high-fidelity semantic distillation generally requires pixel-wise semantic classes. To generate dense semantic maps, we utilize SAM-2 [29], passing in each object class and its associated bounding box. We maintain a dictionary (hash-table), representing the set of objects identified in the image. Now, we can distill the pixel-wise semantic information into the underlying GSplat model. To predict the semantic class of each ellipsoid in the scene, we apply an affine transformation \mathcal{W} to the semantic attribute β of each ellipsoid, mapping β to an N -dimensional space, where N denotes the size of the dictionary. Subsequently, we apply the softmax function to the resulting outputs to define a probability over the entries in the dictionary. We extend this procedure to view-based rendering. Given a camera pose for rendering, we utilize differentiable tile-based rasterization [12] to render a semantic feature map corresponding to the camera pose. We utilize the aforementioned procedure to transform the semantic feature of each pixel to a probability distribution over the entries in the hash-table. We optimize the semantic attributes using the multi-class cross-entropy loss function, given by:

$$\mathcal{L}_{ce} = - \sum_{\mathcal{I} \in \mathcal{D}} \frac{1}{|\mathcal{T}|} \sum_{p \in \mathcal{T}} \gamma_p \log \left(\frac{\exp(\mathcal{F}_{\mathcal{I},p,c})}{\sum_{j=1}^N \exp(\mathcal{F}_{\mathcal{I},p,j})} \right), \quad (3)$$

where \mathcal{T} represents the set of all indices of pixels in the rendered feature map $\mathcal{F}_{\mathcal{I}}$ associated with image \mathcal{I} (after applying the affine transformation \mathcal{W}), c denotes the true class of the pixel, and γ_p represents the weight associated with pixel p . We augment the set of object classes for each view with an *undetected* class label and assign a lower weight to pixels with this class label, i.e., pixels that were not segmented during the data pre-processing phase. This augmentation step serves as a regularization term for the stability of undetected pixels. We train all attributes of the GSplat representation, e.g., the geometric, visual, and semantic attributes and \mathcal{W} ,

simultaneously using the loss function: $\mathcal{L}_{sgs} = \mathcal{L}_{gs} + \mathcal{L}_{ce}$, with \mathcal{L}_{gs} defined in (2).

Open-Vocabulary Semantic Gaussian Splatting. The resulting distillation method enables object localization from a pre-defined set of object classes. However, it does not support open-ended queries from users, which represent an important practical use-case. Here, we extend the capability of the distillation method from the closed-set setting to the open-vocabulary setting, leveraging open-source pre-trained text encoders, e.g., CLIP [27] and BERT [5]. These pre-trained text encoders compute text embeddings for natural language inputs, mapping these inputs to a metric space.

We pre-compute the text embeddings θ_d of each entry in the dictionary of detected object classes using the pre-trained text encoder, without any fine-tuning. At runtime, given a natural-language prompt specified by a user, FAST-Splat computes the text embedding θ_q associated with the prompt using the pre-trained text encoder. To identify semantically-relevant objects in the scene, we compute the *relevancy score* [13], which represents the pairwise softmax between the cosine-similarity values computed over the dictionary embeddings θ_d and a set of text embeddings consisting of the query embedding θ_q (*positive* embedding) and a set of canonical embeddings (*negative* embeddings).

Given a threshold on the relevancy score, we designate all entries whose relevancy score exceeds this specified threshold as being similar to the query. We map these entries to pixels in a rendered feature map using the probability distribution over all entries computed via the softmax function. In general, we can assign a label to each pixel by taking the maximum probability value; however, alternative techniques can be utilized, including multi-hypothesis prediction methods, e.g., conformal prediction [34].

Fine-grained Language Semantics. In the real-world, identifying only the location of a related object of interest, e.g., in semantic object localization, is generally inadequate. Identifying the precise semantic class of the localized object is of even greater importance, especially for downstream applications where semantic object localization constitutes a single component of a solution pipeline. Prior semantic GSplat methods lack this critical capability. For example, existing semantic GSplat methods will localize a coffee machine when a user asks specifically for some “tea,” without disambiguating the semantic identity of the localized object, which could be misleading to a user. FAST-Splat seeks to address this limitation. The novel distillation technique employed by FAST-Splat endows the algorithm with the capability to not only identify the precise semantic class of each object, but also to disambiguate the semantic identity of related objects. Given a natural-language prompt, FAST-Splat identifies the related object classes from its dictionary and subsequently, provides the location of these objects in the scene along with their specific semantic label, illustrated in Figure 1.

5. Experiments

We examine the semantic segmentation and disambiguation capabilities of FAST-Splat, e.g., in scenarios with ambiguous user prompts and scenarios with multiple related objects. We summarize the results here and provide additional implementation details and results in the Supplementary Material.

Baselines. We evaluate FAST-Splat against existing semantic GSplat methods: LangSplat [26] and Feature-3DGS (F-3DGS) [50]. We do not compare our work with FMGS [52], which does not have a publicly-available code implementation. We utilize the original code implementation provided by the authors of these baseline methods.

Datasets and Metrics. We evaluate each method across the benchmark datasets: 3D-OVS [20], LERF [13], and MipNeRF360 [2]. Further, we examine each method in uncurated real-world scenes, e.g., in typical household settings. In each dataset, we report the mean intersection-over-union (mIoU), localization accuracy, and training time [mins].

5.1. Comparison: Benchmark Datasets.

We evaluate all methods on the 3D-OVS dataset, composed of a set of long-tail objects in different backgrounds and poses, and the LERF dataset. Table 1 presents the mIoU scores achieved by each method in the 3D-OVS dataset, with FAST-Splat achieving the highest mIoU in each scene. Specifically, FAST-Splat outperforms LangSplat and F-3DGS by about 8.3% and 40%, respectively, in mIoU. Similarly, from Table 2, FAST-Splat achieves the highest localization accuracy scores, outperforming LangSplat and F-3DGS by about 1.2% and 7.4%, respectively.

Moreover, the novel architecture of FAST-Splat enables significantly faster training, highlighted in Table 3, where FAST-Splat achieves 5.6x and 7.7x speedups in training time compared to LangSplat and F-3DGS, respectively. LangSplat requires two independent training phases for each scene (one for the underlying Gaussian representation and another for the distillation procedure), resulting in significantly longer training times. In addition, LangSplat utilizes costly data pre-processing procedures, making multiple queries to the CLIP and SAM models for semantics extraction, further degrading its computational performance. Similarly, F-3DGS suffers from these challenges. In contrast, FAST-Splat overcomes these challenges with its single-phase training procedure (see Figure 2), resulting in much faster training times. These results underscore the superior performance of FAST-Splat compared to existing methods. In Figure 3, we show the semantic segmentation masks generated by each method. Unlike F-3DGS, which fails to segment many of the objects in the scenes, FAST-Splat and LangSplat provide quite accurate segmentation masks. However, on average, FAST-Splat achieves higher accuracy. We present the results on the LERF dataset in Appendix B.

Table 1. mIoU Scores in the 3D-OVS Dataset.

Scene	LangSplat [26]	F-3DGS [50]	FAST-Splat [Ours]
Bed	0.925	0.643	0.933
Covered-Desk	0.779	0.678	0.913
overall	0.852	0.661	0.923

Table 2. Localization accuracy in the 3D-OVS Dataset.

Scene	LangSplat [26]	F-3DGS [50]	FAST-Splat [Ours]
Bed	0.992	0.961	0.998
Covered-Desk	0.978	0.895	0.995
overall	0.985	0.928	0.997

Table 3. Total training times [mins] in the 3D-OVS Dataset.

Scene	LangSplat [26]	F-3DGS [50]	FAST-Splat [Ours]
Bed	79.23	107.25	13.96
Covered-Desk	78.36	112.06	13.96

5.2. Ablations.

Next, we ablate the choice of using an open-set detector compared to using only a closed-set detector in FAST-Splat using the MipNeRF360 datasets. We use the YOLO model for closed-set object detection. In Tables 4 and 5, we report the mIoU and localization accuracy associated with each approach. From these results, the open-set detector significantly improves the segmentation performance of FAST-Splat beyond that of the closed-set detector. In particular, the open-set detector improves the overall mIoU and localization accuracy scores by about 97% and 25%, respectively, compared to the closed-set detector. This performance boost can be explained by the greater expressiveness of the open-set detector, enabling it to identify varied objects, compared to the relatively limited set of objects that can be identified by a closed-set detector. However, using an open-set detector results in slightly longer training times. The closed-set approach requires about 10.30 mins and 25.73 mins in the *Kitchen* and *Bicycle* scenes, respectively, compared to the open-set approach, which requires about 12.28 mins and 27.82 mins in the *Kitchen* and *Bicycle* scenes. We provide further ablation results, along with renderings of the segmentation masks, using the 3D-OVS and LERF datasets in Appendix C.

Table 4. IoU Scores in MipNeRF360.

Scene	Closed-Set	Open-Set
Kitchen	0.366	0.869
Bicycle	0.395	0.633
overall	0.381	0.751

Table 5. Localization accuracy in MipNeRF360.

Scene	Closed-Set	Open-Set
Kitchen	0.887	0.976
Bicycle	0.577	0.855
overall	0.732	0.916

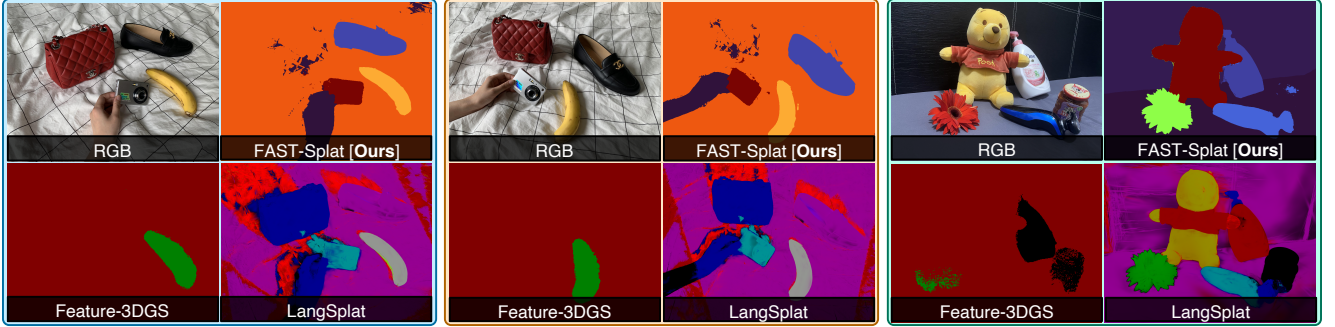


Figure 3. Semantic segmentation on the *Bed* and *Covered-Desk* scenes in 3D-OVS. Overall, FAST-Splat outperforms the baselines.



Figure 4. RGB images rendered in *R-Kitchen* and *R-Library*. FAST-Splat achieves 18x to 51x faster rendering speeds with at least 6x lower memory usage, while achieving competitive or better reconstruction quality.

5.3. Comparison: Uncurated Real-World Datasets.

In addition, we create a dataset of images from uncurated real-world scenes to capture the diversity of objects that would typically occur in real-world scene. We collect data from (i) a home kitchen in its natural, everyday state, comprising the *R-Kitchen* dataset and (ii) a home library, containing books and plants, comprising the *R-Library* dataset. We keep the scale of the training images in the uncurated dataset the same as that of MipNerf360, a widely-used benchmark dataset. We describe the data setup in greater detail in the Appendix A. Here, we examine the fidelity of the 3D scene reconstruction, reporting the structural similarity index measure (SSIM), the peak signal-to-noise ratio (PSNR), the rendering speed in frames per second [FPS], and memory usage [GB] in Table 6. FAST-Splat enables real-time rendering speeds, essentially retaining the performance of the original GSplat work [12], compared to LangSplat and F-3DGS, whose performance is limited by their semantics distillation design. FAST-Splat achieves 51x and 18.8x speedup in rendering speed and the highest SSIM scores compared to the best-competing method, in the *R-Kitchen* and *R-Library* datasets, respectively. LangSplat achieves the highest PSNR score in the *R-Kitchen* dataset, while FAST-Splat achieves

the highest PSNR score in the *R-Library* dataset. Further, FAST-Splat reduces the memory usage by about 7.6x and 6.1x and the training times by about 6.7x and 8.4x, compared to the best competitor in both datasets.

Table 6. The rendering frame-rate (Speed [FPS]), image quality, and memory usage (Memory [GB]) in Uncurated Real-World Datasets.

Method	Speed \uparrow	SSIM \uparrow	PSNR \uparrow	Memory \downarrow
<i>R-Kitchen</i>				
LangSplat [26]	2.25	0.966	35.26	8.05
F-3DGS [50]	0.23	0.931	30.20	7.72
FAST-Splat [ours]	115.23	0.971	34.24	1.02
<i>R-Library</i>				
LangSplat [26]	6.84	0.915	28.79	7.09
F-3DGS [50]	0.21	0.773	25.33	7.72
FAST-Splat [ours]	128.77	0.942	31.12	1.17

Semantic Disambiguation. FAST-Splat extends the capabilities of semantic GSplat methods beyond semantic object localization to the domain of semantic disambiguation. As noted in the preceding discussion, existing semantic GSplat methods cannot resolve semantic ambiguity either arising

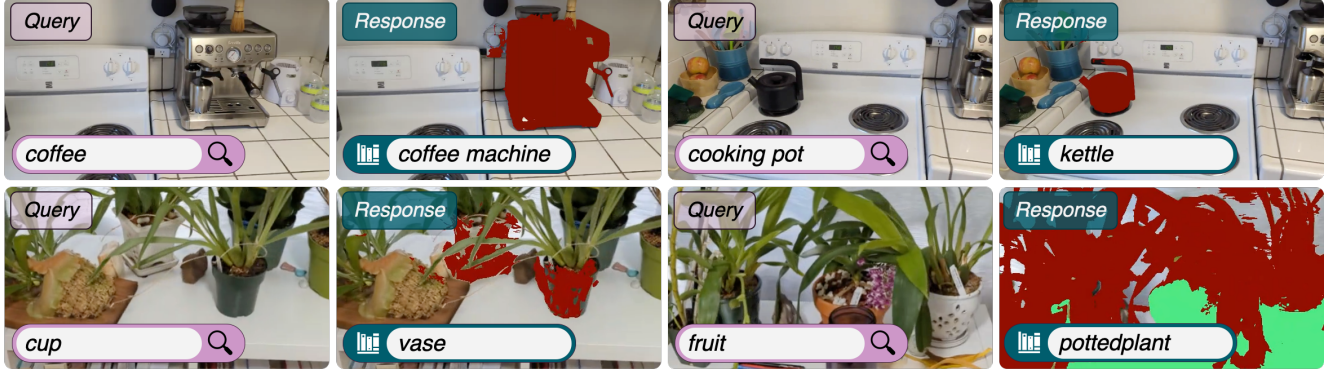


Figure 5. FAST-Splat resolves language ambiguity in natural-language queries in semantic object localization, identifying the specific semantic class of each object, e.g., a *coffee machine* and a *kettle*, when prompted with an ambiguous query, e.g., “coffee” and “cooking pot,” respectively. Likewise, FAST-Splat disambiguates between a “cup” and a *vase* and between a “fruit” and a *pottedplant* in *R-Library*.

Table 7. Total training times [mins] in Uncurated Real-World Datasets.

Scene	LangSplat [26]	F-3DGS [50]	FAST-Splat [Ours]
R-Kitchen	187.03	88.24	13.20
R-Library	199.60	126.91	15.02

from the natural-language query or inherently from the scene composition. In contrast, when provided with an ambiguous natural-language query, FAST-Splat disambiguates the semantic object localization task, by identifying the specific semantic label of related objects in the scene.

We provide some examples in Figure 5. For example, when a user queries for “coffee” in the *R-Kitchen* scene, FAST-Splat provides the user with the semantic identity of the related object, *coffee machine*, along with its semantic segmentation mask and location, given a threshold for the segmentation task. Likewise, when queried for a “cooking pot,” FAST-Splat identifies the semantic class: *kettle*, including its segmentation mask and location. Notably, in the *R-Library* scene, FAST-Splat resolves the ambiguity between a cup and a vase. When queried with the prompt “cup,” FAST-Splat informs the user that, more precisely, a *vase* exists in the scene. Similarly, when asked to localize a “fruit,” FAST-Splat clarifies that the scene contains a *pottedplant* and provides the semantic segmentation mask and location.

Scene Editing. FAST-Splat enables scene-editing of GSplat scenes, by leveraging semantics in Gaussian Splatting. With FAST-Splat, a user can modify the visual properties of a scene, and in addition, insert, delete, or move objects in the scene. For space considerations, we omit a detailed discussion of this capability, given that it has been discussed in prior work. In Figure 6, we provide an example where the color of the *coffee machine* in *R-Kitchen* is modified.



Figure 6. Color-editing of a coffee machine using FAST-Splat.

6. Conclusion

We introduce FAST-Splat, a fast semantic GSplat method that resolves ambiguity in semantic object localization. FAST-Splat retains the explicit form of Gaussian Splatting and avoids neural architectures to achieve fast training and rendering speeds compared to existing methods. FAST-Splat jointly trains the geometric, visual, and semantic attributes of a scene without any neural models, resulting in faster training times, rendering rates. FAST-Splat leverages a hash-table of semantic codes to resolve semantic ambiguity arising from the natural-language query or the scene composition, in the semantic object localization task, addressing one of the fundamental limitations of prior semantic GSplat methods.

7. Limitations and Future Work

FAST-Splat relies on 2D vision-language foundation models, e.g., CLIP, for distilling semantics into GSplat scenes. Hence, the quality of the resulting semantic GSplat depends on the expressiveness of the semantic embeddings computed by the vision-language model. FAST-Splat might fail to recognize objects if the vision-language model fails to correctly identify such objects. Future work will seek to estimate the uncertainty of the semantic embeddings computed by vision-language models to better characterize the limitations of the trained semantic GSplat and ultimately provide safety and performance guarantees for the semantic GSplat.

Acknowledgment

This work was supported in part by NSF project FRR 2342246, and ONR project N00014-23-1-2354, and DARPA project HR001120C0107. Toyota Research Institute provided funds to support this work.

References

- [1] Jonathan T Barron, Ben Mildenhall, Matthew Tancik, Peter Hedman, Ricardo Martin-Brualla, and Pratul P Srinivasan. Mip-nerf: A multiscale representation for anti-aliasing neural radiance fields. In *Proceedings of the IEEE/CVF international conference on computer vision*, pages 5855–5864, 2021. 3
- [2] Jonathan T Barron, Ben Mildenhall, Dor Verbin, Pratul P Srinivasan, and Peter Hedman. Mip-nerf 360: Unbounded anti-aliased neural radiance fields. In *Proceedings of the IEEE/CVF conference on computer vision and pattern recognition*, pages 5470–5479, 2022. 6
- [3] Nicolas Carion, Francisco Massa, Gabriel Synnaeve, Nicolas Usunier, Alexander Kirillov, and Sergey Zagoruyko. End-to-end object detection with transformers. In *European conference on computer vision*, pages 213–229. Springer, 2020. 2, 5
- [4] Boyuan Chen, Fei Xia, Brian Ichter, Kanishka Rao, Keerthana Gopalakrishnan, Michael S Ryoo, Austin Stone, and Daniel Kappler. Open-vocabulary queryable scene representations for real world planning. In *2023 IEEE International Conference on Robotics and Automation (ICRA)*, pages 11509–11522. IEEE, 2023. 3
- [5] Jacob Devlin. Bert: Pre-training of deep bidirectional transformers for language understanding. *arXiv preprint arXiv:1810.04805*, 2018. 5, 12
- [6] Jacob Devlin, Ming-Wei Chang, Kenton Lee, and Kristina Toutanova. Bert: Pre-training of deep bidirectional transformers for language understanding. In *North American Chapter of the Association for Computational Linguistics*, 2019. 3
- [7] Alexey Dosovitskiy. An image is worth 16x16 words: Transformers for image recognition at scale. *arXiv preprint arXiv:2010.11929*, 2020. 2
- [8] Xiuye Gu, Tsung-Yi Lin, Weicheng Kuo, and Yin Cui. Open-vocabulary object detection via vision and language knowledge distillation. *arXiv preprint arXiv:2104.13921*, 2021. 3
- [9] Kaiming He, Georgia Gkioxari, Piotr Dollár, and Ross Girshick. Mask r-cnn. In *Proceedings of the IEEE international conference on computer vision*, pages 2961–2969, 2017. 2
- [10] Xu Hu, Yuxi Wang, Lue Fan, Junsong Fan, Junran Peng, Zhen Lei, Qing Li, and Zhaoxiang Zhang. Semantic anything in 3d gaussians. *arXiv preprint arXiv:2401.17857*, 2024. 3, 4
- [11] Chenguang Huang, Oier Mees, Andy Zeng, and Wolfram Burgard. Visual language maps for robot navigation. In *2023 IEEE International Conference on Robotics and Automation (ICRA)*, pages 10608–10615. IEEE, 2023. 3
- [12] Bernhard Kerbl, Georgios Kopanas, Thomas Leimkühler, and George Drettakis. 3d gaussian splatting for real-time radiance field rendering. *ACM Trans. Graph.*, 42(4):139–1, 2023. 3, 4, 5, 7, 12
- [13] Justin Kerr, Chung Min Kim, Ken Goldberg, Angjoo Kanazawa, and Matthew Tancik. Lrf: Language embedded radiance fields. In *Proceedings of the IEEE/CVF International Conference on Computer Vision*, pages 19729–19739, 2023. 1, 2, 3, 4, 5, 6
- [14] Diederik P. Kingma and Jimmy Ba. Adam: A method for stochastic optimization. *CoRR*, abs/1412.6980, 2014. 4, 12
- [15] Sossuke Kobayashi, Eiichi Matsumoto, and Vincent Sitzmann. Decomposing nerf for editing via feature field distillation. *Advances in Neural Information Processing Systems*, 35:23311–23330, 2022. 2, 3, 4
- [16] Boyi Li, Kilian Q Weinberger, Serge Belongie, Vladlen Koltun, and René Ranftl. Language-driven semantic segmentation. *arXiv preprint arXiv:2201.03546*, 2022. 1, 3
- [17] Feng Li, Hao Zhang, Huaizhe Xu, Shilong Liu, Lei Zhang, Lionel M Ni, and Heung-Yeung Shum. Mask dino: Towards a unified transformer-based framework for object detection and segmentation. In *Proceedings of the IEEE/CVF Conference on Computer Vision and Pattern Recognition*, pages 3041–3050, 2023. 3
- [18] Liunian Harold Li, Pengchuan Zhang, Haotian Zhang, Jianwei Yang, Chunyuan Li, Yiwu Zhong, Lijuan Wang, Lu Yuan, Lei Zhang, Jenq-Neng Hwang, et al. Grounded language-image pre-training. In *Proceedings of the IEEE/CVF Conference on Computer Vision and Pattern Recognition*, pages 10965–10975, 2022. 3
- [19] Feng Liang, Bichen Wu, Xiaoliang Dai, Kunpeng Li, Yinan Zhao, Hang Zhang, Peizhao Zhang, Peter Vajda, and Diana Marculescu. Open-vocabulary semantic segmentation with mask-adapted clip. In *Proceedings of the IEEE/CVF Conference on Computer Vision and Pattern Recognition*, pages 7061–7070, 2023. 3
- [20] Kunhao Liu, Fangneng Zhan, Jiahui Zhang, Muyu Xu, Yingchen Yu, Abdulmotaleb El Saddik, Christian Theobalt, Eric Xing, and Shijian Lu. Weakly supervised 3d open-vocabulary segmentation. *Advances in Neural Information Processing Systems*, 36:53433–53456, 2023. 6
- [21] Quande Liu, Youpeng Wen, Jianhua Han, Chunjing Xu, Hang Xu, and Xiaodan Liang. Open-world semantic segmentation via contrasting and clustering vision-language embedding. In *European Conference on Computer Vision*, pages 275–292. Springer, 2022. 3
- [22] Shilong Liu, Zhaoyang Zeng, Tianhe Ren, Feng Li, Hao Zhang, Jie Yang, Chunyuan Li, Jianwei Yang, Hang Su, Jun Zhu, et al. Grounding dino: Marrying dino with grounded pre-training for open-set object detection. *arXiv preprint arXiv:2303.05499*, 2023. 3, 5
- [23] Ben Mildenhall, Pratul P Srinivasan, Matthew Tancik, Jonathan T Barron, Ravi Ramamoorthi, and Ren Ng. Nerf: Representing scenes as neural radiance fields for view synthesis. *Communications of the ACM*, 65(1):99–106, 2021. 3
- [24] Matthias Minderer, Alexey Gritsenko, Austin Stone, Maxim Neumann, Dirk Weissenborn, Alexey Dosovitskiy, Aravindh Mahendran, Anurag Arnab, Mostafa Dehghani, Zhuoran Shen, et al. Simple open-vocabulary object detection. In *European Conference on Computer Vision*, pages 728–755. Springer, 2022. 1, 3

- [25] Thomas Müller, Alex Evans, Christoph Schied, and Alexander Keller. Instant neural graphics primitives with a multi-resolution hash encoding. *ACM transactions on graphics (TOG)*, 41(4):1–15, 2022. [3](#)
- [26] Minghan Qin, Wanhua Li, Jiawei Zhou, Haoqian Wang, and Hanspeter Pfister. Langsplat: 3d language gaussian splatting. In *Proceedings of the IEEE/CVF Conference on Computer Vision and Pattern Recognition*, pages 20051–20060, 2024. [2](#), [3](#), [4](#), [6](#), [7](#), [8](#), [12](#)
- [27] Alec Radford, Jong Wook Kim, Chris Hallacy, Aditya Ramesh, Gabriel Goh, Sandhini Agarwal, Girish Sastry, Amanda Askell, Pamela Mishkin, Jack Clark, et al. Learning transferable visual models from natural language supervision. In *International conference on machine learning*, pages 8748–8763. PMLR, 2021. [1](#), [2](#), [3](#), [5](#), [12](#)
- [28] Adam Rashid, Satvik Sharma, Chung Min Kim, Justin Kerr, Lawrence Yunliang Chen, Angjoo Kanazawa, and Ken Goldberg. Language embedded radiance fields for zero-shot task-oriented grasping. In *7th Annual Conference on Robot Learning*, 2023. [2](#), [3](#)
- [29] Nikhila Ravi, Valentin Gabeur, Yuan-Ting Hu, Ronghang Hu, Chaitanya Ryali, Tengyu Ma, Haitham Khedr, Roman Rädle, Chloe Rolland, Laura Gustafson, et al. Sam 2: Segment anything in images and videos. *arXiv preprint arXiv:2408.00714*, 2024. [1](#), [3](#), [5](#)
- [30] N Reimers. Sentence-bert: Sentence embeddings using siamese bert-networks. *arXiv preprint arXiv:1908.10084*, 2019. [3](#)
- [31] Shaoqing Ren, Kaiming He, Ross Girshick, and Jian Sun. Faster r-cnn: Towards real-time object detection with region proposal networks. *IEEE transactions on pattern analysis and machine intelligence*, 39(6):1137–1149, 2016. [2](#)
- [32] Tianhe Ren, Shilong Liu, Ailing Zeng, Jing Lin, Kunchang Li, He Cao, Jiayu Chen, Xinyu Huang, Yukang Chen, Feng Yan, et al. Grounded sam: Assembling open-world models for diverse visual tasks. *arXiv preprint arXiv:2401.14159*, 2024. [3](#)
- [33] Johannes Lutz Schönberger and Jan-Michael Frahm. Structure-from-motion revisited. In *Conference on Computer Vision and Pattern Recognition (CVPR)*, 2016. [12](#)
- [34] Glenn Shafer and Vladimir Vovk. A tutorial on conformal prediction. *Journal of Machine Learning Research*, 9(3), 2008. [5](#)
- [35] Nur Muhammad Mahi Shafiullah, Chris Paxton, Lerrel Pinto, Soumith Chintala, and Arthur Szlam. Clip-fields: Weakly supervised semantic fields for robotic memory. *arXiv preprint arXiv:2210.05663*, 2022. [1](#), [3](#)
- [36] William Shen, Ge Yang, Alan Yu, Jansen Wong, Leslie Pack Kaelbling, and Phillip Isola. Distilled feature fields enable few-shot language-guided manipulation. *arXiv preprint arXiv:2308.07931*, 2023. [2](#), [3](#)
- [37] Ola Shorinwa, Johnathan Tucker, Aliyah Smith, Aiden Swann, Timothy Chen, Roya Firoozi, Monroe Kennedy III, and Mac Schwager. Splat-mover: Multi-stage, open-vocabulary robotic manipulation via editable gaussian splatting. *arXiv preprint arXiv:2405.04378*, 2024.
- [38] Ola Shorinwa, Jiankai Sun, Mac Schwager, and Anirudha Majumdar. Siren: Semantic, initialization-free registration of multi-robot gaussian splatting maps. *arXiv preprint arXiv:2502.06519*, 2025. [3](#)
- [39] Matthew Tancik, Ethan Weber, Evonne Ng, Ruilong Li, Brent Yi, Terrance Wang, Alexander Kristoffersen, Jake Austin, Kamyar Salahi, Abhik Ahuja, et al. Nerfstudio: A modular framework for neural radiance field development. In *ACM SIGGRAPH 2023 Conference Proceedings*, pages 1–12, 2023. [12](#)
- [40] Can Wang, Menglei Chai, Mingming He, Dongdong Chen, and Jing Liao. Clip-nerf: Text-and-image driven manipulation of neural radiance fields. In *Proceedings of the IEEE/CVF Conference on Computer Vision and Pattern Recognition*, pages 3835–3844, 2022. [2](#), [3](#), [4](#)
- [41] Chien-Yao Wang, I-Hau Yeh, and Hong-Yuan Mark Liao. Yolov9: Learning what you want to learn using programmable gradient information. In *European Conference on Computer Vision*, pages 1–21. Springer, 2025. [5](#)
- [42] Weiyao Wang, Matt Feiszli, Heng Wang, Jitendra Malik, and Du Tran. Open-world instance segmentation: Exploiting pseudo ground truth from learned pairwise affinity. In *Proceedings of the IEEE/CVF conference on computer vision and pattern recognition*, pages 4422–4432, 2022. [3](#)
- [43] Zhuyu Yao, Jiangbo Ai, Boxun Li, and Chi Zhang. Efficient detr: improving end-to-end object detector with dense prior. *arXiv preprint arXiv:2104.01318*, 2021. [5](#)
- [44] Jiahui Yu, Zirui Wang, Vijay Vasudevan, Legg Yeung, Mojtaba Seyedhosseini, and Yonghui Wu. Coca: Contrastive captioners are image-text foundation models. *arXiv preprint arXiv:2205.01917*, 2022. [1](#)
- [45] Alireza Zareian, Kevin Dela Rosa, Derek Hao Hu, and Shih-Fu Chang. Open-vocabulary object detection using captions. In *Proceedings of the IEEE/CVF Conference on Computer Vision and Pattern Recognition*, pages 14393–14402, 2021. [3](#)
- [46] Hao Zhang, Feng Li, Shilong Liu, Lei Zhang, Hang Su, Jun Zhu, Lionel M Ni, and Heung-Yeung Shum. Dino: Detr with improved denoising anchor boxes for end-to-end object detection. *arXiv preprint arXiv:2203.03605*, 2022. [2](#), [3](#)
- [47] Hao Zhang, Feng Li, Xueyan Zou, Shilong Liu, Chunyuan Li, Jianwei Yang, and Lei Zhang. A simple framework for open-vocabulary segmentation and detection. In *Proceedings of the IEEE/CVF International Conference on Computer Vision*, pages 1020–1031, 2023. [3](#)
- [48] Youcai Zhang, Xinyu Huang, Jinyu Ma, Zhaoyang Li, Zhaochuan Luo, Yanchun Xie, Yuzhuo Qin, Tong Luo, Yaqian Li, Shilong Liu, et al. Recognize anything: A strong image tagging model. In *Proceedings of the IEEE/CVF Conference on Computer Vision and Pattern Recognition*, pages 1724–1732, 2024. [5](#)
- [49] Yuhang Zheng, Xiangyu Chen, Yupeng Zheng, Songen Gu, Runyi Yang, Bu Jin, Pengfei Li, Chengliang Zhong, Zengmao Wang, Lina Liu, et al. Gaussiangrasper: 3d language gaussian splatting for open-vocabulary robotic grasping. *arXiv preprint arXiv:2403.09637*, 2024. [3](#)
- [50] Shijie Zhou, Haoran Chang, Sicheng Jiang, Zhiwen Fan, Zehao Zhu, Dejia Xu, Pradyumna Chari, Suyu You, Zhangyang

- Wang, and Achuta Kadambi. Feature 3dgs: Supercharging 3d gaussian splatting to enable distilled feature fields. In *Proceedings of the IEEE/CVF Conference on Computer Vision and Pattern Recognition*, pages 21676–21685, 2024. 2, 3, 4, 6, 7, 8, 12
- [51] Xingyi Zhou, Rohit Girdhar, Armand Joulin, Philipp Krähenbühl, and Ishan Misra. Detecting twenty-thousand classes using image-level supervision. In *European Conference on Computer Vision*, pages 350–368. Springer, 2022. 1
- [52] Xingxing Zuo, Pouya Samangouei, Yunwen Zhou, Yan Di, and Mingyang Li. Fmgs: Foundation model embedded 3d gaussian splatting for holistic 3d scene understanding. *International Journal of Computer Vision*, pages 1–17, 2024. 3, 4, 6

Appendix A. Implementation Details

To implement FAST-Splat, we build off Splatfacto in Nerfstudio [39], and utilize the text encoder of the OpenAI’s CLIP ResNet model *RN50x64* [27] to compute the text embeddings. However, other text encoders can also be used, e.g., other CLIP models or BERT [5]. We train FAST-Splat using Stochastic Gradient Descent with momentum, via the Adam optimizer [14].

For the uncurated real-world datasets, we collected the training data by taking videos of the scene using a smartphone camera. We utilized structure-from-motion, e.g., COLMAP [33], for computing the pose of the camera for each frame used in training the GSplat model. FAST-Splat is trained on an NVIDIA GeForce RTX 3090 GPU with 24GB VRAM for 30000 iterations, using the hyperparameters specified in [39] in its Splatfacto model. We train the baseline methods LangSplat and Feature-3DGS using the original code implementation provided by their respective authors on an NVIDIA GeForce RTX 3090 Ti GPU with 24GB VRAM, giving LangSplat and Feature-3DGS an advantage on hardware, since the 3090 Ti has 10752 CUDA cores compared to the 10496 CUDA cores on the 3090, among other improved hardware specifications. To train LangSplat, we follow the procedure provided by its authors, which involves pre-training the Gaussian Splatting Scene using the code implementation provided in [12], prior to training the semantic components. We do not include the structure-from-motion processing times in any of the results reported in the experiments, given that this procedure is required universally by all methods.

Appendix B. Comparison on the LERF Dataset

We provide additional results on the segmentation performance of each method in the LERF dataset. In Tables 8 to 10, we provide the mIoU and localization accuracy scores achieved by FAST-Splat, LangSplat, and F-3DGS. FAST-Splat achieves the highest overall mIoU score and localization accuracy and achieves the highest localization accuracy in each scene. F-3DGS achieves the highest mIoU score in the *Ramen* and *Waldo_kitchen* scenes, while FAST-Splat achieves the highest mIoU scores in the *Teatime* and *Waldo_kitchen* scenes. From Table 10, FAST-Splat requires significantly shorter training times compared to the baselines, providing 7.7x, 6.9x, and 7.5x speedups compared to the best-competing methods in the *Ramen*, *Teatime*, and *Waldo_kitchen* scenes, respectively. These results further highlight the superior performance of FAST-Splat compared to existing baselines.

Appendix C. Ablations.

Further, we discuss ablation results in the 3D-OVS and LERF datasets, where we evaluate the performance of FAST-Splat

Table 8. mIoU Scores in the LERF Dataset.

Scene	LangSplat [26]	F-3DGS [50]	FAST-Splat [Ours]
Ramen	0.512	0.600	0.566
Teatime	0.651	0.613	0.706
Waldo_kitchen	0.445	0.533	0.533
overall	0.536	0.582	0.602

Table 9. Localization accuracy in the LERF Dataset.

Scene	LangSplat [26]	F-3DGS [50]	FAST-Splat [Ours]
Ramen	0.732	0.876	0.935
Teatime	0.881	0.890	0.972
Waldo_kitchen	0.955	0.863	0.971
overall	0.856	0.876	0.959

Table 10. Total training times [mins] in the LERF Dataset.

Scene	LangSplat [26]	F-3DGS [50]	FAST-Splat [Ours]
Ramen	141.98	116.49	15.08
Teatime	175.26	114.53	16.70
Waldo_kitchen	189.55	123.77	16.59

with only a closed-set detector and the variant with an open-set detector. Tables 11 and 12 provide the mIoU and localization accuracy scores for the closed-set and open-set approaches in the 3D-OVS dataset. In this dataset, the open-set approach improves the mIoU score by about 8.8x and the localization accuracy by about 1.9x relative to that of the closed-set approach. In Figures 7 and 8, we show the segmentation masks produced by each approach. The closed-set approach fails to produce meaningful segmentation masks in the *Bed* scene; in contrast, the open-set approach produces highly-accurate segmentation masks. The closed-set approach performs better in the *Covered-Desk* scene (relative to the *Bed* scene), localizing the teddy bear. However, the closed-set approach fails when segmenting long-tail objects such as the *gerbera* in Figure 8, which the open-set approach successfully localizes.

We observe similar findings in the LERF dataset in Tables 14 and 15, where the open-set approach improves the mIoU and localization accuracy scores by about 2x and 1.15x. Figures 9 and 10 shows the segmentation masks generated by each approach. While the closed-set approach fails to produce highly-detailed segmentation masks, e.g., segmenting the egg, noodles, and pork-belly in the bowl, the open-set approach provides higher-fidelity segmentation masks. Likewise, the closed-set approach fails to distinguish the sheep from the teddy bear in Figure 10, unlike the open-set approach. However, in all the datasets, the closed-set approach requires shorter training times compared to the open-set approach.

Lastly, in Figure 11, we provide a few segmentation im-



Figure 7. Semantic segmentation on the *Bed* scene in 3D-OVS. Whereas the closed-set approach fails to produce high-quality segmentation masks, the open-set approach achieves high accuracy.

ages generated by the closed-set and open-set approaches in the MipNerf360 datasets. Although the closed-set approach fails to accurately segment the bicycle behind the bench, the open-set approach successfully segments the bicycle. These results underscore the importance of the open-set detector in FAST-Splat.

Table 11. mIoU Scores in the 3D-OVS Datasets.

Scene	Closed-Set	Open-Set
Bed	0.044	0.933
Covered-Desk	0.165	0.913
overall	0.105	0.923

Table 12. Localization accuracy in the 3D-OVS Datasets.

Scene	Closed-Set	Open-Set
Bed	0.165	0.998
Covered-Desk	0.893	0.995
overall	0.529	0.997



Figure 8. Semantic segmentation on the *Covered-Desk* in 3D-OVS. The open-set approach achieves higher accuracy, especially for long-tail objects, e.g., the *gerbera* (a daisy/flower).

Table 13. Total training times [mins] in the 3D-OVS Datasets.

Scene	Closed-Set	Open-Set
Bed	12.6	13.96
Covered-Desk	12.07	13.96

Table 14. mIoU Scores in the LERF Datasets.

Scene	Closed-Set	Open-Set
Ramen	0.135	0.566
Teatime	0.407	0.706
Waldo_kitchen	0.343	0.533
overall	0.295	0.602

Table 15. Localization accuracy in the LERF Datasets.

Scene	Closed-Set	Open-Set
Ramen	0.736	0.935
Teatime	0.916	0.972
Waldo_kitchen	0.858	0.971
overall	0.837	0.959

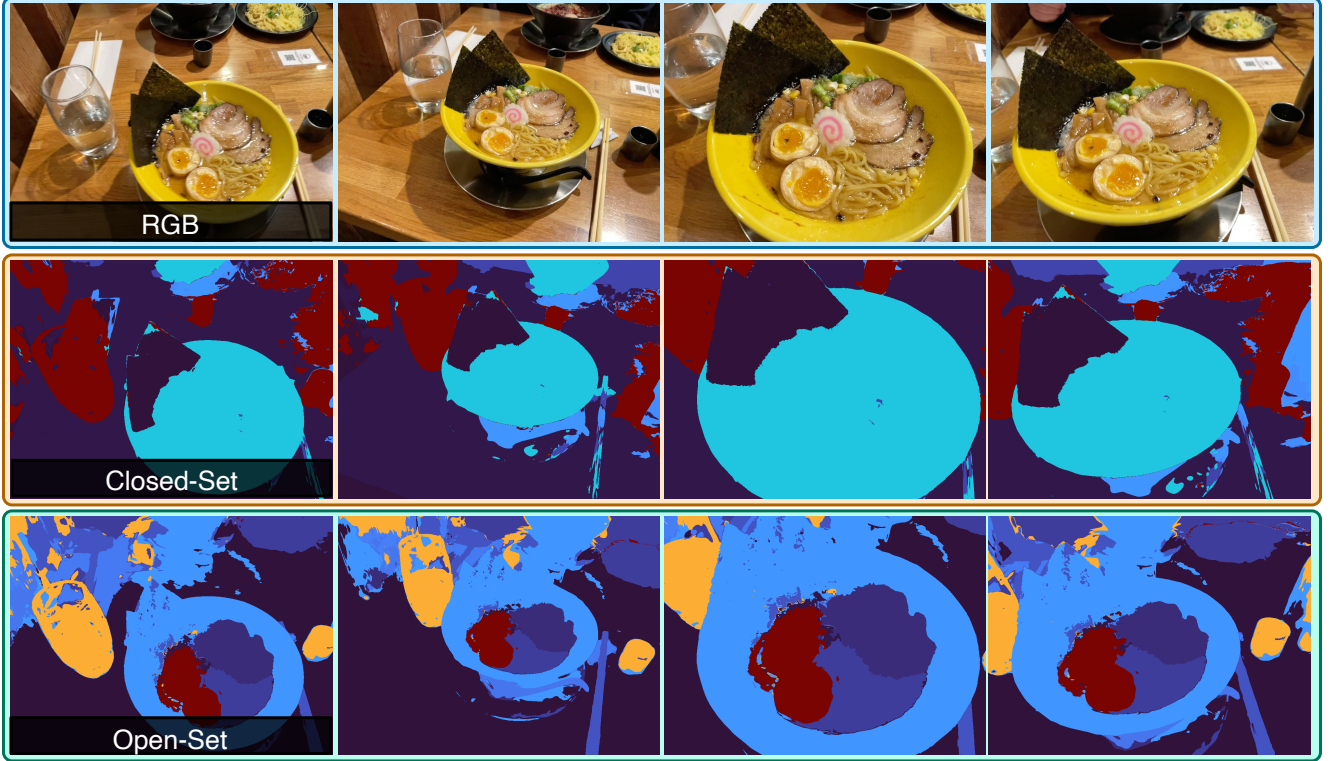


Figure 9. Semantic segmentation of the *Ramen* scene in the LERF dataset. The closed-set approach fails to generate highly-detailed segmentation masks, unlike the open-set approach.



Figure 10. Semantic segmentation of the *Teatime* scene in the LERF dataset. The closed-set achieves a relatively better segmentation performance compared to other scenes, but fails to distinguish between the sheep and the teddy bear.

Table 16. Total training times [mins] in the LERF Datasets.

Scene	Closed-Set	Open-Set
Ramen	13.86	15.08
Teatime	15.01	16.70
Waldo_kitchen	13.99	16.59

Appendix D. Semantic Object Localization

Here, we provide additional results, demonstrating the photorealistic novel-view synthesis capability of FAST-Splat, including its semantic segmentation masks. In Figure 12, we show the semantic localization of a “wall,” “countertop,” “kettle,” and “cooking spoon.” In each case, FAST-Splat successfully localizes the pertinent object. The colors in each figure vary with the similarity of the object to the natural-language query. We utilize the “Turbo” colormap, with an

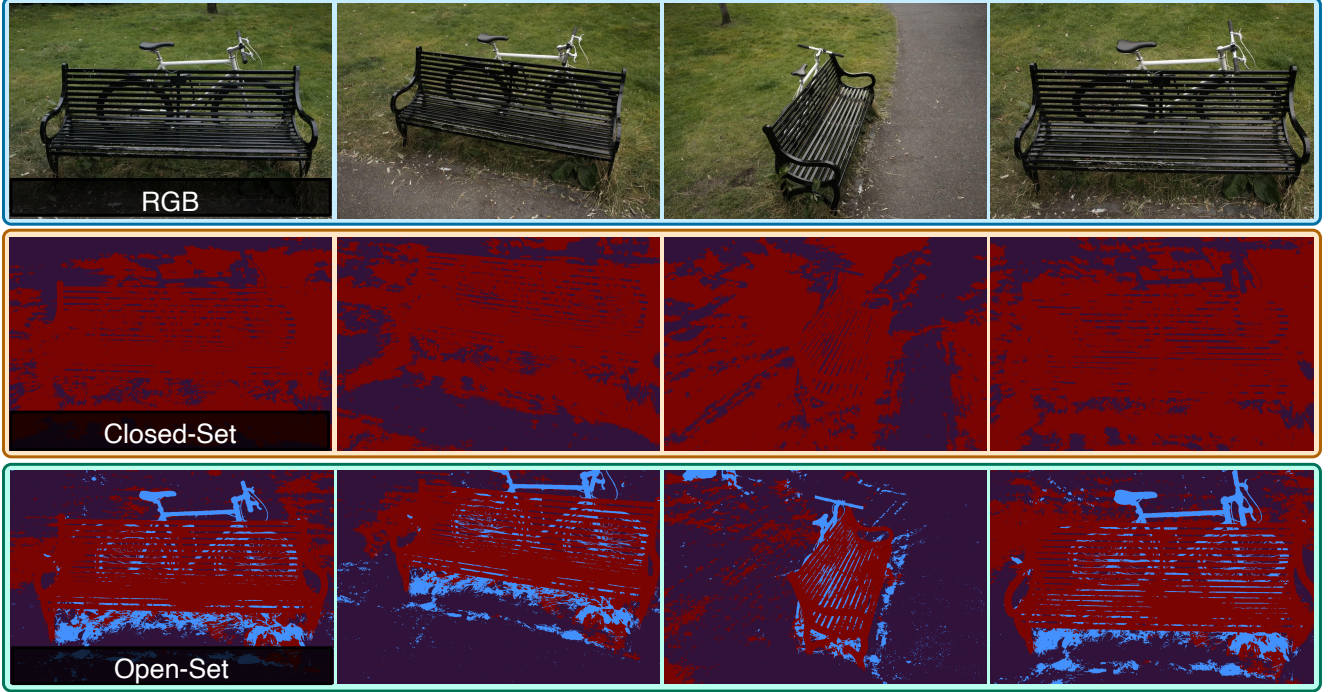


Figure 11. Semantic segmentation of the *Bicycle* scene in the MipNerf360 dataset. The closed-set approach fails to accurately segment the bicycle behind the bench, unlike the open-set approach.

increase in the intensity of the red color channel indicating an *increase* in the similarity of an object to the query and an increase in the intensity of the blue color channel indicating a *decrease* in the relevance of an object to the query, in general. Moreover, the RGB images rendered by FAST-Splat appear photorealistic, displayed in the top row in Figure 12, all rendered at novel views.

prompt.

Appendix E. Semantic Disambiguation

As discussed earlier in this work, FAST-Splat enables semantic disambiguation, e.g., in semantic object localization. Not only does FAST-Splat provide the semantic identity of the most relevant object, FAST-Splat also identifies other pertinent objects, providing the semantic label of these objects along with their similarity to the natural-language prompt. In Figure 13, we demonstrate the semantic disambiguation capabilities of FAST-Splat. In the top row, when queried for a “fork,” FAST-Splat identifies the *spoon* as the object that is most similar to the query. In addition, FAST-Splat localizes the *knife*, identifying it as being relevant, although less similar, compared to the spoon. Likewise, in the bottom row, when prompted with the ambiguous query “water,” FAST-Splat localizes the *kettle*, noting its lower similarity compared to a *coffee machine*, which FAST-Splat also localizes in the scene. Lastly, FAST-Splat identifies the *bottle* as the most similar object to the query, resolving the ambiguous

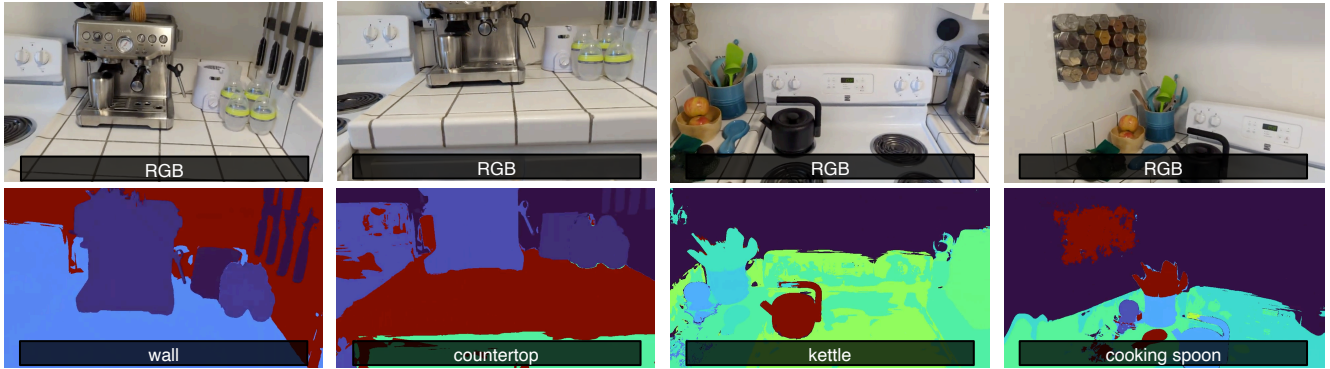


Figure 12. FAST-Splat enables semantic object localization with open-vocabulary user prompts. Here, we provide segmentation results for a “wall,” “countertop,” “kettle,” and “cooking spoon.”



Figure 13. FAST-Splat resolves semantic ambiguity in object localization from natural-language queries. In the top row, although the queried object “fork” does not exist in the scene, FAST-Splat localizes relevant objects in the scene, and more importantly, provides the semantic label of each of these objects. Here, FAST-Splat identifies a *spoon* and a *knife* and notes that the spoon (not the knife) is more similar to the fork. Likewise, in the bottom row, given the ambiguous prompt “water,” FAST-Splat localizes a *kettle*, *coffee machine*, and *bottle*, providing their semantic object classes along with their relative similarity to the prompt.